OBSERVATIONS OF THE 24 SEPTEMBER 1997 CORONAL FLARE WAVES

B. J. THOMPSON[1], B. REYNOLDS[2], H. AURASS[3], N. GOPALSWAMY[4], J. B. GURMAN[5], H. S. HUDSON[6], S. F. MARTIN[7] and O. C. ST. CYR[8]
[1]*NASA Goddard Space Flight Center, Greenbelt, MD, U.S.A.*
[2]*Perth, Australia*
[3]*Astrophysikalisches Institut Potsdam, Potsdam, Germany*
[4]*Catholic University of America, Washington, DC, U.S.A.*
[5]*NASA Goddard Space Flight Center, Greenbelt, MD, U.S.A.*
[6]*Solar Physics Research Corp., Tucson, AZ, U.S.A.*
[7]*Helio Research, La Crescenta, CA, U.S.A.*
[8]*Computational Physics Inc., Fairfax, VA, U.S.A.*

(Received 20 September 1999; accepted 8 November 1999)

Abstract. We report coincident observations of coronal and chromospheric 'flare wave' transients in association with a flare, large-scale coronal dimming, metric radio activity and a coronal mass ejection. The two separate eruptions occurring on 24 September 1997 originate in the same active region and display similar morphological features. The first wave transient was observed in EUV and Hα data, corresponding to a wave disturbance in both the chromosphere and the solar corona, ranging from 250 to approaching 1000 km s^{-1} at different times and locations along the wavefront. The sharp wavefront had a similar extent and location in both the EUV and Hα data. The data did not show clear evidence of a driver, however. Both events display a coronal EUV dimming which is typically used as an indicator of a coronal mass ejection in the inner corona. White-light coronagraph observations indicate that the first event was accompanied by an observable coronal mass ejection while the second event did not have clear evidence of a CME. Both eruptions were accompanied by metric type II radio bursts propagating at speeds in the range of 500$-$750 km s^{-1}, and neither had accompanying interplanetary type II activity. The timing and location of the flare waves appear to indicate an origin with the flaring region, but several signatures associated with coronal mass ejections indicate that the development of the CME may occur in concert with the development of the flare wave.

1. Introduction

Metric type II radio bursts have normally been taken to be the manifestation of a shock wave propagating in the solar corona (Uchida, 1960; Wild, Smerd, and Weiss, 1963; Weiss, 1965). An MHD shock wave excites plasma radiation, by accelerating electrons and creating an energized population which serves as the source of the radio bursts (e.g., Wild, Sheridan, and Neylan, 1959; Smith, 1972; review by Mann, 1995). Their association with flares was quickly established, and several authors, including Maxwell and Thompson (1962), demonstrated that the initiation time of type II bursts corresponded extremely well with the timing of the

Solar Physics **193:** 161–180, 2000.

associated flare. However, Dodson, Hedeman, and Chamberlain (1953) performed a study which led them to conclude that metric radio bursts were more clearly associated with high-velocity ejections than solar flares. Roberts (1959) followed this up by stating that the majority of flares of any magnitude range are not accompanied by type II activity, implying that an additional condition must be present for the radio bursts to form. Compelling arguments for and against the possible candidates for this special condition have been developed.

The problem with the 'high-velocity ejecta' or 'piston-driven' shock idea was that the estimated speeds of the shocks exceeded most of the candidate drivers. To resolve this discrepancy, Wagner and MacQueen (1983) proposed that for a flare to be accompanied by type II activity, the flare blast wave must overtake a density enhancement or CME. Uchida and co-authors (Uchida, Altschuler, and Newkirk, 1973; Uchida, 1974) noted that an MHD wave produced by a flare or other exciting impulse could steepen into a shock, which could excite Langmuir turbulence and high-frequency radio emission. Uchida's mechanism allowed for a weak MHD fast-mode wave to produce metric type II bursts, without requiring the continued presence of a piston to drive the wave. The debate over the 'piston-driven' vs 'blast wave' origin of shock waves continues today, as detailed in a review by Cliver, Webb, and Howard (1999, and references therein).

The development of several of the models of type II radio burst production occurred in conjunction with studies of rapidly moving phenomena on the Sun which were presumed to be solar shock waves or the manifestations of solar shock waves. Studies prior to 1961 focused on 'action at a distance' by a flare, such as sympathetic flaring (e.g., Richardson, 1936, 1951) and the report of the initiation of filament oscillations during a flare by Dodson (1949). The report of Moreton (1960), Moreton and Ramsey (1960) and Athay and Moreton (1961) of arc-shaped transients quickly ($>$1000 km s^{-1}) sweeping through the corona observed in Hα images was swiftly incorporated into the study of radio burst production. Authors such as Wild, Smerd, and Weiss (1963) proposed that these 'flare waves' or 'Moreton waves' could have the same origin as the radio type II bursts, and Kai (1970) demonstrated a strong relationship between the waves and the radio bursts. Studies such as those in Smith and Harvey (1971) demonstrated that the timing of the flare wave initiation corresponded well with the flare, and that the associated radio type II activity commenced in parallel with the wave observations.

Based on the morphology of the waves and estimates of coronal magnetic field and density, Meyer (1968) deduced that the waves probably were fast MHD disturbances in nature, and endeavored to explicitly determine the coronal magnetic field using these considerations. Uchida (1968) further developed this notion by considering the refraction of such a wave, and performed simulations which reproduced the location of the chromospheric disturbance through the initiation of a three-dimensional coronal disturbance. The correspondence was more compelling as the radio observations were incorporated into the model.

Pinter (1977) reported that 70% of the flare waves reported in his study were accompanied by type II radio bursts, and argued that the correlation could be much higher, as the association appeared to improve as the number and sensitivity of ground-based radio observations improved. Pinter found that the estimated speed of the radio observations exceeded, but were typically proportional to, the associated flare wave velocities.

Thompson *et al.* (1998, 1999) detailed the observation of coronal wave transients which were candidates for the coronal counterpart of the chromospheric observations. Because there were no associated Hα observations of Moreton waves, and because of several differences (most notably their slow speed, quasi-isotropic propagation, and diffuse morphology) from the sharp, arc-shaped Hα waves, the phenomena were labeled 'EIT waves' (after SOHO/EIT, the observing instrument) in anticipation of more definitive observations.

Klassen *et al.* (2000) extended the results of previous flare wave and radio correlative studies by performing a similar study with the 'EIT wave' transients. They found a strong association between Potsdam type II radio bursts and the EUV activity as observed by SOHO/EIT. The survey found at least 90% of the radio type II bursts had associated EUV activity indicative of an 'EIT wave' transient. Individual studies by Klassen *et al.* (1999) and Pick *et al.* (1999) have added to our understanding of the correspondence between radio and coronal observations. Other authors, such as Torsti *et al.* (1999) and Krucker *et al.* (1999) investigated correlations between these waves and interplanetary particle events.

Despite these studies, which indicated strong associations between 'EIT wave' observations and phenomena which had previously been linked to flare waves as well, the timing and location of the 'EIT waves' indicated that it was very possible that they could be driven by coronal mass ejections. Although the observations were not thorough enough to exclude flares as a driver of the EUV waves, the development of CME-associated features in conjunction with the waves introduced additional complexity into the study.

Cliver, Webb, and Howard (1999) performed a study of metric type II bursts and CMEs observed during the Solar Maximum Mission, and found that the correlation between the two phenomena increased dramatically as the origin of the radio activity approached the solar limb. They went on to argue that since the correlation appeared to improve with the visibility of the CME (i.e., as the CME launch angle approached the solar limb), the type II bursts had a more clear association with CMEs. Furthermore, this association improved remarkably if the speed of the CME exceeded 400 km s^{-1}. Because of the prior connection that was made between metric type II bursts and flare waves, Cliver, Webb, and Howard further favored a strong flare wave/CME correspondence. It became clear that the coronal observations were essential to unravel the mystery of what drives coronal shock waves.

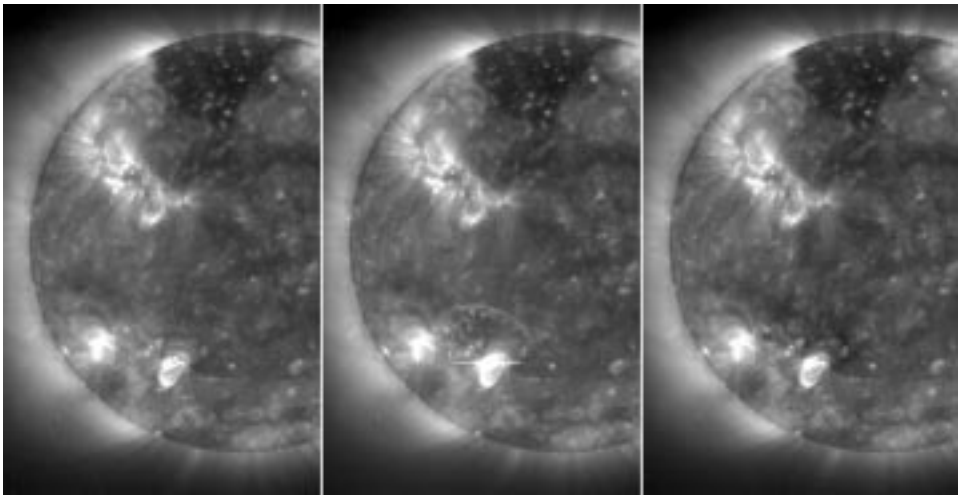

Figure 1. Subfields of SOHO/EIT 195 Å images at 02:33, 02:49 and 03:03 UT on 24 September 1997, showing the eastern portion of the Sun during the development of the first event.

2. Coronal Observations

In this study we examine two EIT waves associated with two M-class flares with GOES peak times at 02:48 UT (M5.9) and 11:06 UT (M3.0) respectively. Neither event had complete hard X-ray coverage either from the Compton Gamma Ray Observatory or from the *Yohkoh* spacecraft, but for the first event Hα observations are available as well, and for the second event coronal metric radio burst data are discussed.

The Extreme ultraviolet Imaging Telescope (EIT) (Delaboudinière *et al.*, 1995) images the solar disk and inner corona of the Sun in four pass bands consisting of strong EUV spectral lines. The observations in this paper consist of a wavelength range which is centered on 195 Å, as the three other wavelength regimes are obtained at a much lower cadence and were not available for the times we discuss. The primary wavelengths observed with the 195 Å pass band are FeXII 192.3, 193.5 and 195.1 Å. The temperature at which these emissions peak at coronal densities is approximately 1.5–1.6 MK. Images are recorded on a 1024 $\times$ 1024 pixel (44.2 $\times$ 44.2 arc min) EUV-sensitive CCD camera, with a pixel size of 2.59 arc sec.

EIT was running a campaign consisting of full-disk 195 Å images consisting of a single half-resolution image every 10–23 min. A 'pre-event' image is shown in the first frame of Figure 1, restricted to the eastern portion of the image, where the activity is observed. The first frame of Figure 1 was recorded at 02:33 UT, while the second and third frames were recorded at 02:49 and 03:03 UT. NOAA active region No. 8088 is visible in the southeast at a heliographic location of S28, E20, while NOAA region No. 8087 was positioned to the east at S25, E45. The complex containing active region No. 8089 was located to the north ranging N10 to N45

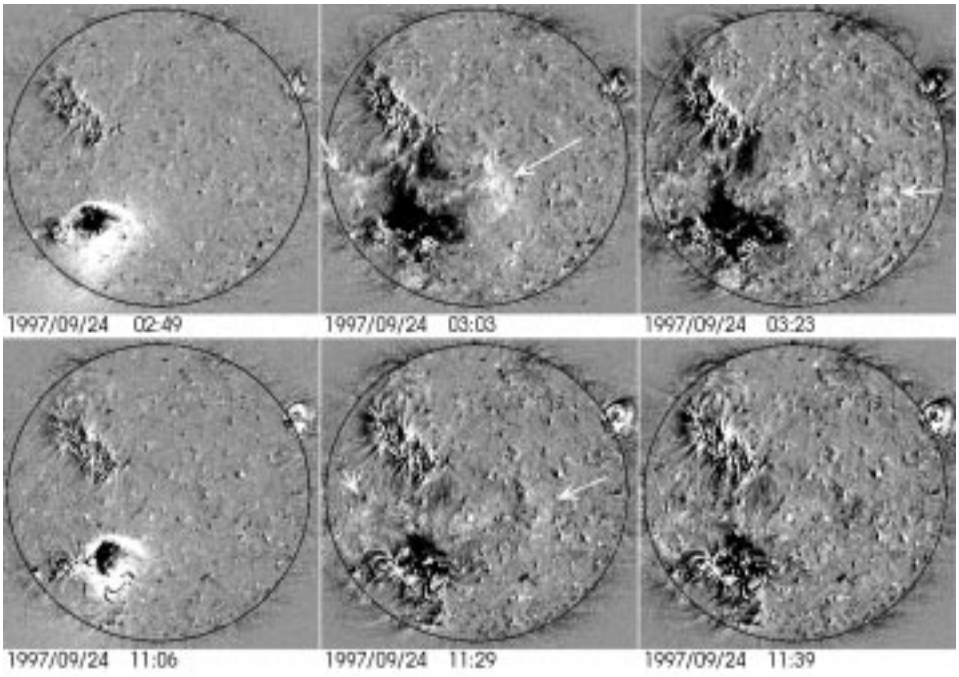

Figure 2. Differenced SOHO/EIT images for the two events on 24 September 1997. The first row of images, recorded at 02:49, 03:03 and 03:23 UT, have a pre-event image at 02:33 UT digitally subtracted from them. The second set of images (11:06, 11:29 and 11:39 UT) had an image at 10:46 UT subtracted from each. The arrows indicate the progression of the weak wavefront.

and from E20 to near the observable limb. Two features of the sequence are worth noting. First, a comparison of the first and third images reveals a large degree of decreased emission to the north of AR No. 8088, to the northeast of AR No. 8087, and to the south of AR No. 8089. Also, the same image pair displays a relatively low degree of evolution observed to the south of the flaring region No. 8088. Most of the evidence of this eruption in the EUV are confined to regions north of the flaring region and south of AR No. 8089. An exception is the center image, near the time of the flare, when a broad increase in emission is observed over an area roughly five arc min in diameter centered on the flare; this is assumed to be due primarily to scattered light in the instrument as a result of the flare (F. Auchere, personal communication). Otherwise, the most dramatic changes occur to the north of the flaring region.

To illustrate this point more clearly, a series of differenced images are shown in Figure 2 for the eruptions beginning at 02:49 UT and at 11:06 UT. Each image has a 'pre-event' image subtracted from it; for the first set of images (02:49, 03:03 and 03:23 UT) the image at 02:33 UT was digitally subtracted from each one to enhance changes occurring in the corona. The second set of images (11:06, 11:29 and 11:39 UT) had an image at 10:46 UT subtracted from each. These 'pre-event'

images were the last images recorded before clear evidence of the eruptions was observed. Therefore they also serve as a lower limit to the times in which various aspects of the eruption developed.

The series of images shows a strong correspondence between the two separate eruptions. Both start off with a sharp, compact bright front propagating northward from region No. 8088 and extending over an angle of approximately 120 degrees. The bright front in the first (02:49 UT) panel of Figure 2 is also visible in the middle EIT image in Figure 1. The horizontal line in this frame corresponds to an instrumental artifact of the flare resulting from a local overfilling of CCD pixels. The bright front exhibits an average increase of more than 100 %, with small ($<$20 arc sec) areas exceeding a 200 % increase.

For context, Figure 3 shows the local evolution of the two eruptions. The middle row of two figures are subfields of EIT images at 02:49 and 03:03 UT, and the lower two figures are subfields from 11:06 and 11:29 UT. The top row shows larger subfields of images from the *Yohkoh* Soft X-ray Telescope (SXT) obtained at 02:35 and 03:51 UT. The first image was obtained at a quarter of the SXT resolution and the second at a half, both with the Aluminum Magnesium (AlMg) filter. A single SXT pixel spans 2.46 arc sec. The portion of the brightening extending to the north of the flaring region in the 03:51 UT SXT image is an instrumental artifact due to the brightness of the flaring region. The GOES soft X-ray photometer observed a flare of magnitude M5.9 beginning at 02:43 UT, peaking at 02:48 UT, and ending at 02:52 UT. The later event was associated with an M3.0 flare from 10:57–11:10 UT, peaking at 11:06 UT. Although the BATSE instrument on the Compton Gamma Ray Observatory was not observing at the time of the first flare, BATSE recorded a hard X-ray flare beginning at 1107:17 UT and peaking at 1107:33 UT in association with the later event.

The SXT images indicate that additional loop structures either brightened or became visible following the flare and eruption. The loops, marked by arrows in Figure 3, formed primarily to the immediate north of the flaring region, while there was some evidence of a new soft X-ray loop spanning the equator extending from region No. 8088 to No. 8089. The SXT images were not obtained at a sufficient cadence to show the development of these features. These features are typically identified as signatures of a large-scale magnetic reconfiguration usually associated with a coronal mass ejection (Rust, 1983; Hudson, Acton, and Freeland, 1996; Hudson and Webb, 1997; Nitta and Akiyama, 1999). A ‘cusp-shaped’ feature, extending to the south from the same region, is formed before the event takes place and shows little sign of evolution during the event, indicating that it was perhaps independent of it.

The bright front and the EUV flare both appear in the same image for both events (02:49 UT and 11:06 UT); based on the EUV observations alone, the low cadence of the images make it impossible to determine which originated first. Another phenomenon first appears in these images as well, a dark region between the flaring region and the bright front. This dark ‘dimming’ region remains for a

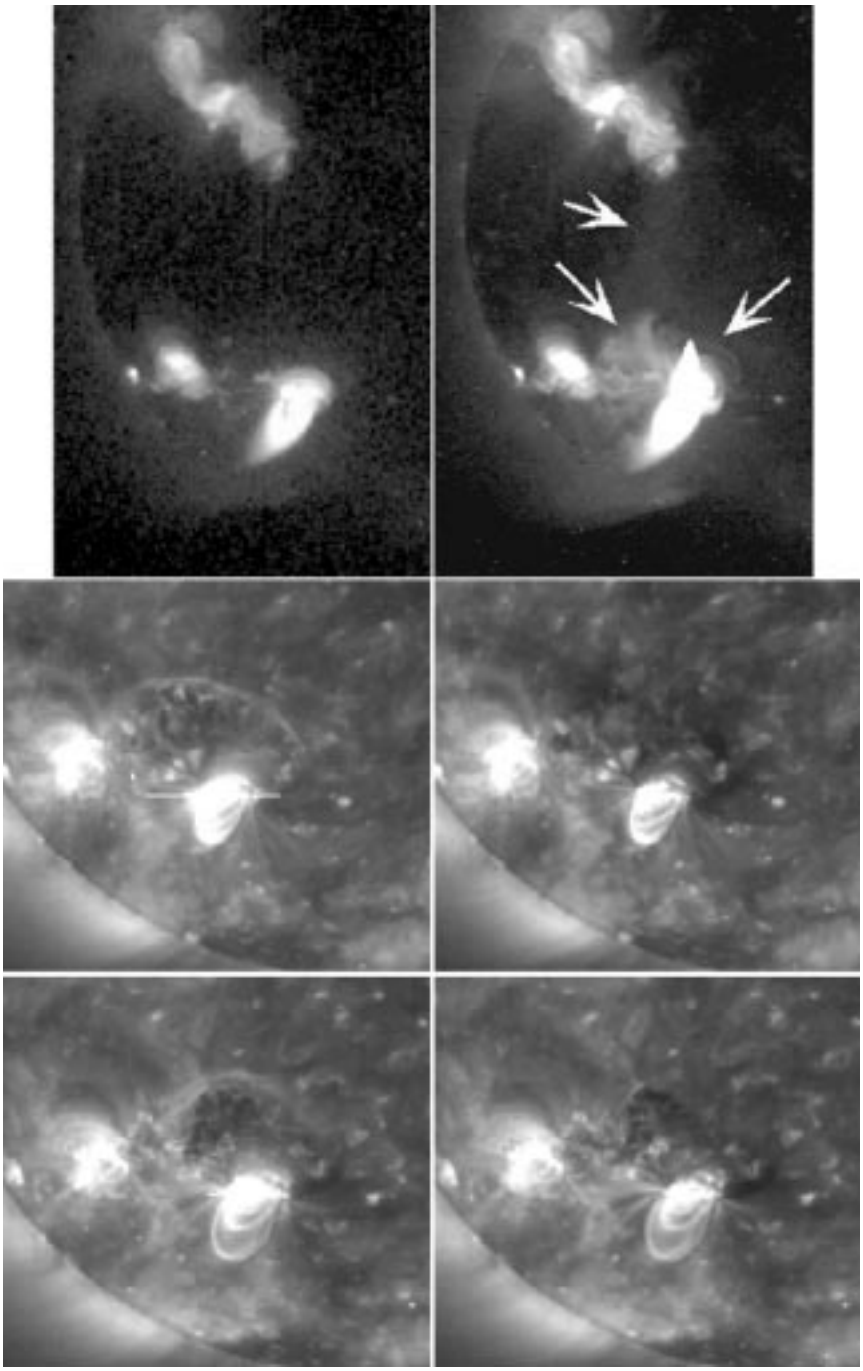

Figure 3. The top row shows larger subfields of images from the *Yohkoh* Soft X-ray Telescope (SXT) obtained at 02:35 and 03:51 UT, detailing the development of the first eruption. The middle row are subfields of EIT images at 02:49 and 03:03 UT, and the lower two figures are subfields from 11:06 and 11:29 UT. Each pair shows the development of the eruption close to the flaring site; a sharp bright arc is visible in the 02:49 and 11:06 EIT images.

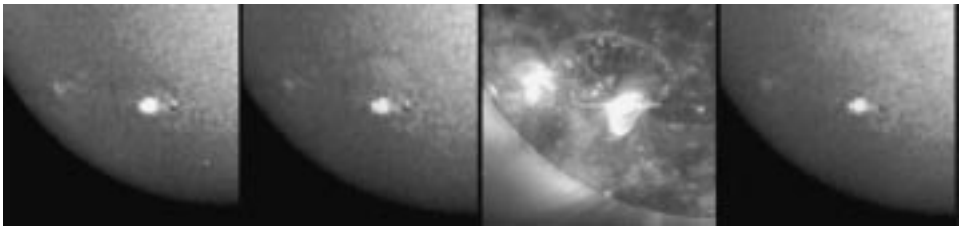

Figure 4. Hα images of the first eruption obtained at 02:45, 02:47 and 02:50 UT. The corresponding EIT sub-frame at 02:49:21 UT is shown in the third frame of the figure.

fairly long duration (>8 hours) and consists of a decrease of 30–40% on average, exceeding 50% in small (<20 arc sec) regions.

The dimming region develops gradually, appearing only up to the sharp wavefront in the images at 02:49 and 11:06 UT, but extending over greater distances towards active region No. 8089 in later images. The relative lack of evolution observed north of the wavefront in the images at 02:49 and 11:06 UT, compared to the drastic changes following, indicates that the dimming region and wavefront developed in conjunction.

The difference images in Figure 2 show evidence of the later development of a more diffuse wavefront, most notable in the image at 03:03 UT. A faint bright front (marked by arrows) appears to the east and west of the dimming region, and the total emission increase of less than 20% and the broad expanse are more characteristic of the 'EIT wave' transients described by Thompson *et al.* (1998, 1999). Unlike the sharp propagation fronts, the weaker fronts tend to propagate through the corona and leave very little evidence of their transit which can be observed with the EIT image cadence. Wills-Davey and Thompson (1999) describe the transit of a similar diffuse wave in TRACE EUV data, and discuss the observable local effects. Running-difference images (images with the immediately previous image subtracted from them) and movies show later evidence of the wave (marked by an arrow in Figure 2) at 03:23 near the west limb of the Sun.

3. Hα and Metric Radio Observations

Figure 4 shows Hα observations obtained in conjunction with the EIT observations of the first eruption. The Hα images were obtained with a Vixen 102ED refractor stopped down to 63 mm and a Daystar 0.5 heated T scanner with a 2$\times$ Barlow lens. Exposures of $\frac{1}{125}$ s were recorded on Tech Pan 2415 film. The times of the first, second and fourth frames of Figure 4 were approximately 02:45, 02:47, and 02:50 UT. The corresponding EIT sub-frame at 02:49:21 UT is shown in the third frame of the figure.

The development of the wavefront in the Hα images appears to indicate that the EUV wave and Hα waves are relatively cospatial. These data show a dark,

roughly concentric wavefront propagating outwards from the flare site, similar to early Moreton wave observations. A more diffuse, slightly brightened area follows the dark Hα wavefront, typical of the Doppler shifting into the red wings of the Hα passband as the chromosphere relaxes following the passage of the wave. Another Hα image obtained at 02:55 UT showed no further evidence of the wavefront. Unfortunately, neither the timing of the Hα observations nor that of the EIT observations are accurate to the degree required to properly determine speed estimates; the Hα times are accurate to approximately 30 s, while the EIT times are slightly more accurate. For this reason, it is not possible to determine whether the location of the EUV front leads that of the Hα wavefront, or if they are cospatial. Additionally, it is impossible to determine the altitude at which the EUV emission is being produced, based on the assumption that the EUV emission could be coronal in origin while the Hα emission would be primarily chromospheric. However, the images indicate that the EUV and Hα observations are approximately cospatial.

Figure 5 illustrates the locations of the Hα and EUV wavefronts, assuming that the reported observation times are accurate and that the wavefronts observed in the EUV and Hα are cospatial. The active regions are outlined and the shaded region corresponds to the area which exhibited EUV dimming. The four arcs drawn within the shaded region correspond to the Hα and EUV observations of the sharp wavefront. The line running north-south to the left of the dimming region indicates the location of the farthest edge of the diffuse EUV brightening at 03:03 UT, and the lines running north-south to the right of the dimming region correspond to the location of the diffuse front at 03:03 and 03:23 UT. Five lines are drawn radially from the flare site, as a means of sampling the wave speed at various locations. These lines we will identify as Track 1 through Track 5, numbered from the left to the right.

Assuming the reported observation times are accurate, we compute the speeds along the five tracks. The three data points along Track 1 yield speeds (beginning with the pair closest to the flaring region) of 620 and 630 km s^{-1}, where the speeds correspond to the distance traveled along a great circle on a sphere of one solar radius. The speeds along Track 2 are 430 and 720 km s^{-1}, along Track 3 are 360, 330, and 1000 km s^{-1}, along Track 4 are 380, 280, 1220 and 460 km s^{-1}, and along Track 5 are 310, 410, 1000, 390, and 260 km s^{-1}. The speeds of 1000 and 1220 km s^{-1} correspond to measurements made between the EIT observation at 02:49:21 UT and the Hα observation at 02:50 UT. The large inhomogeneity represented by these speeds indicates two possible difficulties: either the EUV observations are not cospatial with the Hα observations, or the inaccuracy of the observation times is grossly influencing the speed estimates. The speed estimates along Tracks 2-5 based solely on the location of the Hα images at 02:47 and 02:50 UT are 510, 424, 570 and 530 km s^{-1}. This implies that either the reported time of the EIT image at 02:49:21 UT is later than the true observation time, or that the EUV wavefront location leads the location of the Hα wavefronts. The error in the speed estimates is primarily due to the difficulty in determining the

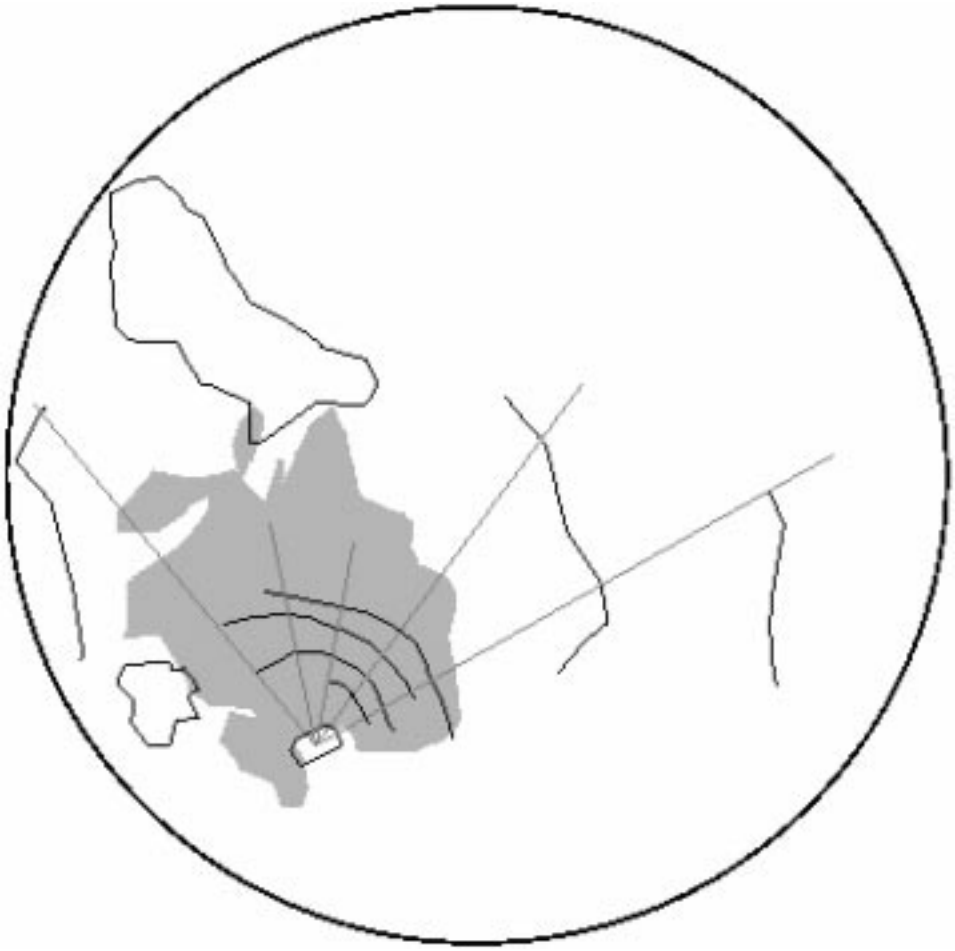

Figure 5. Drawing of the locations of the Hα and EUV wavefronts, corresponding to the wave progression at 02:45, 02:47, 02:49, 02:50, 03:03 and 03:23 UT. The active regions correspond to the black outlines and the shaded region corresponds to the area which exhibited EUV dimming. Five lines are drawn emanating from the flare site, identified from left to right as Track 1 through Track 5.

exact location of the wavefronts and due to timing errors; most of the estimates are probably not accurate to within 25%.

The speed and locations of the wavefront appear to indicate that a plausible origin intersects the flaring site at close to 02:43 UT. The GOES flux was observed to be increasing at this time, and peaked later at 02:48 UT.

Metric radio observations of the eruptions were obtained with the radio spectral polarimeter at the Potsdam Astrophysical Institute (Mann *et al.*, 1992) and with the Hiraiso Radio Spectrograph (HiRAS) in Japan. The Hiraiso observations indicate that a metric type II radio burst began around 02:49 UT (although a type III burst

beginning around 02:47 UT would have obscured any earlier type II activity) and ended at approximately 02:59 UT. Based on the model of Mann *et al.* (1999), the speed of the type II burst was estimated to be approximately 620 km s^{-1}.

The second event was accompanied by type II bursts observed by the Potsdam Astrophysical Institut. This event is reported in a survey by Klassen *et al.* (2000) of the association between Potsdam type II radio bursts and EUV activity as observed by SOHO/EIT. The survey found at least 90% of the radio type II bursts had associated EUV activity indicative of an 'EIT wave' transient. Figure 6 shows the radio observations developing in conjunction with the second EUV event. The EIT observations indicated that activity developed between 10:46 and 11:06 UT. The type II activity associated with this event had several stages. Based on the Mann *et al.* (1999) model, the frequency of the bursts between 11:03:30 and 11:05:30 was relatively constant, indicating that the direction of propagation was transverse to the density gradient. The frequency drift of the 11:07:30 to 11:09:00 bursts was also slight. From 11:05:30 to 11:08:00 and 11:09:00 to 11:13:00 the estimated speed of the burst was approximately 510 km s^{-1}.

Alternative models can cause the estimated speeds to vary; Klassen *et al.* (2000) used the model described by Newkirk (1961) to estimate the speed at 740 km s^{-1} later in the event. Both bursts display several type II lanes and split bands, indicating the disturbance is meeting with many sites of comparatively low magnetic field. The estimated speed of the EUV disturbance, based on the 11:06 and 11:29 UT EIT images, was approximately 200 km s^{-1} to the east and 300 km s^{-1} to the west. If the earlier wave transient at 02:45 UT can be compared to the later event, it is understandable that the speeds obtained with the 11:06 and 11:29 images will be quite slow, as the fastest speeds generally were observed early in the wave's motion, when it had a sharper profile. Klassen *et al.* found a similar result in their catalog: when the wave speeds were determined exclusively using EIT data, the average speed of the type II bursts was nearly three times that of the EIT speeds. However, as seen in the earlier event at 02:45 UT, the speed of the wave based on the Hα observations averaged more than 500 km s^{-1}, which is closer to the estimated type II speed of 620 km s^{-1}. Additionally, the speed determined by the radio bursts represents the speed along a density gradient, while the Hα (and apparently the early EUV) wavefront remains at low altitudes.

4. The Correspondence with a Coronal Mass Ejection

Figure 7 illustrates a series of SOHO/LASCO C2 (Brueckner *et al.*, 1995) images of the coronal mass ejection associated with the first eruption on 24 September 1997, first appearing in the C2 field of view at 03:38 UT. The mass ejection is indicated with arrows in the southeast in the 03:38 UT image and over a 180-deg expanse in a later image at 04:20 UT. Its speed, based on the brightest portion in the southeast in the 03:38 and 04:20 UT images, is estimated to be between

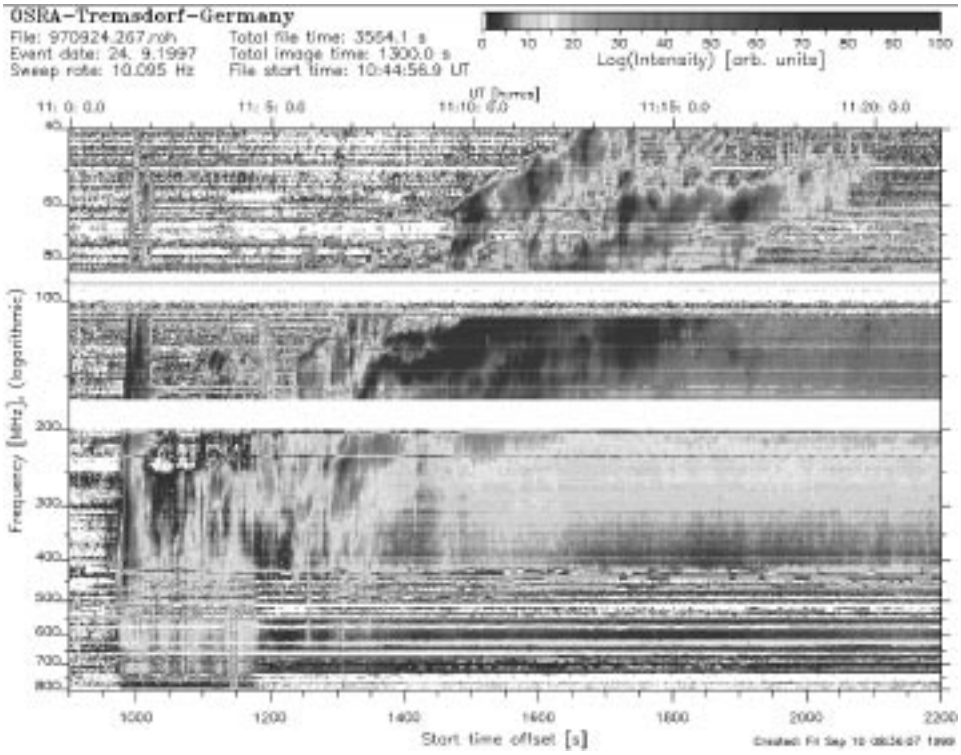

Figure 6. Metric radio data from the second event observed by the radio spectral polarimeter at the Potsdam Astrophysical Institut. Based on the frequency drift of the radio bursts, the speed in the corona was estimated to be between 500 and 750 km s^{-1}.

280 and 350 km s^{-1}. The CME was not visible in the 02:55 UT image, indicating that the leading portion of the CME in the 03:38 UT image was traveling at least 300 km s^{-1}.

The eruption is difficult to observe for several possible reasons. The southeast limb was the site of continuous coronal mass ejections throughout 24 September 1997. At least six mass ejections were observed to the south and southeast, including the loop eruption which was in progress in the southeast in all frames of Figure 7. The mass ejection appearing at 03:38 UT is only seen as a superposition over the existing loop eruption, and is therefore difficult to track.

Another reason the coronal mass ejection was difficult to observe was because of its launch angle. As mentioned previously, the coronal dimming observed in the EUV by SOHO/EIT occurred primarily on the solar disk. As demonstrated by Thompson *et al.* (2000), the white-light extent of a coronal mass ejections corresponds most strongly with the large-scale dimming observed in the EUV images (if such a large-scale dimming is observed). Therefore, most of the CME material would presumably have been launched at an angle of greater than 50 deg from the plane of the sky. The Thomson scattering angle of the material associated with this

eruption would not allow the CME to be as visible as an eruption occurring near the solar limb, as was the case for the earlier loop CME in the southeast.

The brightness of the CME associated with the first eruption in our study is not unusually weak for a 'halo' coronal mass ejection. The 6 January 1997 (Webb *et al.*, 1998) halo coronal mass ejection had roughly the same brightness as the one discussed here. However, the second event commencing around 11:00 UT was accompanied by little or no white light activity (another loop eruption to the southeast was in progress during this event as well). The extent of the EUV dimming was much less than the first eruption, but no systematic study has been done investigating any possible correlation between the EUV or soft X-ray coronal dimming and the white-light brightness of a mass ejection. Studies of halo coronal mass ejections observed by SOHO/LASCO (St. Cyr *et al.*, 1999, and references therein) indicate that the majority of CMEs occurring along the Earth–Sun axis are observed by SOHO/LASCO, inferring that very few mass ejections are 'missed' by LASCO.

The WAVES instrument on board the WIND spacecraft (Bougeret *et al.*, 1995) did not observe interplanetary type II activity with either event (M.L. Kaiser, personal communication). It is not rare that a series of metric radio type II bursts not be accompanied by interplanetary type II bursts (e.g., Robinson, Stewart, and Cane, 1984) but it is still difficult to determine the similarities and differences between their origins (e.g., Gopalswamy *et al.*, 1998; Cliver, 1999). It is generally accepted that the presence of interplanetary type II activity is a strong indicator of a coronal mass ejection (e.g., Cane, 1983).

Additionally, it is important to note that the SOHO and WIND spacecraft, which were both obtaining *in-situ* observations of the solar wind for the days following the eruptions, observed no clear evidence of a disturbance of solar origin (N. Fox, personal communication).

5. Discussion

The Hα observations of the 'flare wave' or 'Moreton wave' beginning at 02:45 on 24 September 1997 correspond well with previous observations of these disturbances, as first reported by Moreton (1960) and Moreton and Ramsey (1960), and as summarized in Smith and Harvey (1971) and Pinter (1977). The wave develops into a discrete arc spanning approximately 120 degrees, and propagates at speeds ranging from a few hundred to over a thousand km s^{-1} (though the highest speed estimates are suspicious due to the unavailability of exact image times). The Hα observations consisted of a dark front propagating from a flare site, with evidence of a brightening following closely behind it. The event is strongly reminiscent of the images taken in Hα + 0.5 Å on 20 September 1963 (Moreton, 1965; Figure 4 of Smith and Harvey, 1971). The 24 September 1997 Hα observations may have contained contributions from the red and blue wings of Hα, commensurate with

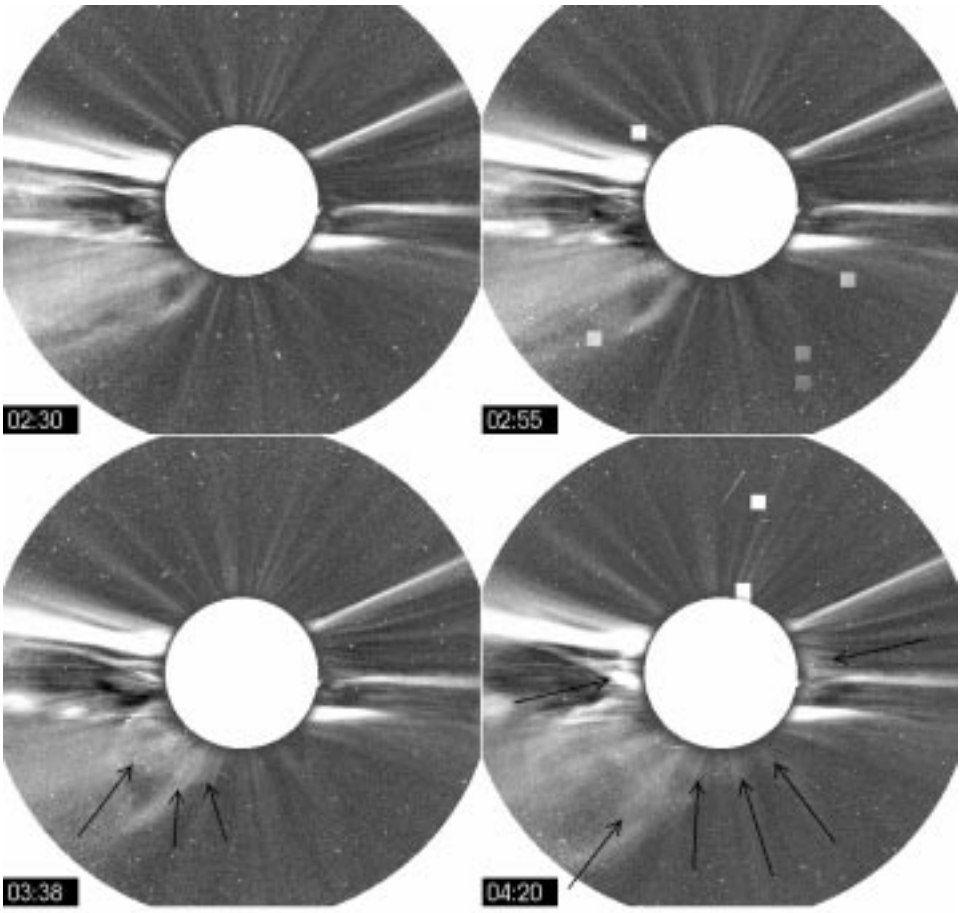

Figure 7. SOHO/LASCO C2 images of coronal mass ejections on 24 September 1997. A CME is in progress in the southeast (lower left) portion of the image, and a second disturbance (indicated by arrows) begins at 03:38 UT.

the interpretation that the wavefront consists of a chromospheric compression followed by relaxation. However, Athay and Moreton (1961) discuss the visibility of these waves in both on-band and in the wings of Hα. Additionally, Smith and Harvey (1971) indicate that some of the wave observations consist of moving material and not just compressional motions; the resolution of the data prohibited a determination of the relative contributions of material motion and chromospheric depression.

The range of frequencies of the observed type II bursts is similar to those reported in the summaries mentioned above, and the type II bursts and wave transient originate at close to the same time. The estimated type II burst velocity is slightly greater than the measured velocity of the chromospheric/coronal disturbance, also concurring with observations of prior flare wave transients. It is fortunate that these

observations are not unusual for a flare wave, as the incorporation of the coronal observations into this phenomenon may be valid for most of these transients.

This study was initiated for two reasons: to examine the coronal counterpart of flare wave transients, and to utilize the broader variety of available data as a means of differentiating between initiators and drivers of these waves. Sadly, only the first of these two goals was accomplished. Both the CME and the flare seem integral to our observations. Additionally, the data are not sufficient to differentiate between different models proposed to explain the early Hα and metric radio data; even with the increased range of data available, we are still left with many of the same questions.

Fortunately, the EUV and Hα observations fairly overlap. Although it was not clear whether the EUV and Hα waves were exactly cospatial, it was clear that they appeared roughly in the same location and had very similar morphologies. The EIT observation of a sharp wavefront at 02:49:21 UT showed a simple correspondence with the Hα data, confirming suspicions that the chromospheric observations of the waves were a manifestation of a phenomenon that was coronal in origin.

Two additional aspects are brought into the study when the coronal observations are incorporated. First, a strong 'coronal dimming' is observed in association with the wave's development, and this, combined with the *Yohkoh* SXT and SOHO/LASCO observations, indicate the possible presence of a coronal mass ejection. Additionally, in later images, a diffuse transient appears which is more typical of the 'EIT waves' discussed earlier. It is impossible to determine from the data available whether the later appearance of a weak 'EIT wave' corresponded with the disappearance of the sharp EUV emission front. This would enable observers to determine whether the two had an associative correspondence, and whether the two were two separate phenomena or are manifestations of the same. It is possible that the sharp coronal fronts, which appear to correspond to potential observability in chromospheric Hα, represent the high-amplitude limit of the weak 'EIT wave' observations. The waves could be more strongly driven or could be steeper during the early stages, and become freely propagating or weaker in its subsequent development.

Nearly all of the EIT wave transients reported in the Klassen *et al.* (2000) study were weak and diffuse and did not have the morphology of the Hα waves. The timing of the Klassen *et al.* events indicated that the radio bursts occurred early in the production of the EIT wave transients. This may imply that the EIT wave transients occur in two stages: an earlier, possibly driven stage, and a later, freely propagating weaker stage. It is conceivable that the weak, quasi-isotropic waves observed in EIT could take on a sharper and more rapidly propagating form in the early stages of propagation, or in the strongly driven limit (thereby resolving the discrepancy in morphology), but there is still a question of the initiator or driver.

The first event showed evidence of an eruption in the LASCO C2 white-light coronagraph data, while the second event was lacking a white light counterpart. Both the EIT and SXT observations had what is usually interpreted as evidence

of a mass ejection in both events, but the studies establishing these signatures were developed in conjunction with white light observations of CMEs. The CME may have been directed far from the plane of the sky, and therefore was not easily observable against a background of steadily evolving corona. If that is not the case, the reliability of the coronal disk signatures comes into question.

The timing and location of the flare relative to the Hα wave transient are similar to early observations; the initiation of the wave appears to be centered on the flare. However, it is possible to propose the CME as the driver of the wave, with the flare serving as an associated (but not initiating) phenomenon. The co-temporal appearance of the coronal dimming may support this explanation. Indeed, the coincident appearance and parallel development of the dimming region and the bright front imply an association, but causality is difficult to determine. The gradual formation of the dark depleted region could represent an expanding driver of the bright front, with the dimming region (CME) causing the bright front to form. Conversely, the bright front could sweep through the ambient corona, causing a drastic change in its wake. It is difficult to believe that a disturbance as strong as the one shown in the wavefront would result in no change in coronal emission; one would expect that heating or cooling out of the EUV 195 Å band pass could easily result. However, the long duration (>3 hours in both cases) and the fairly stable nature of the emission depletion exceeds most estimates of the time it would take for the coronal plasma to return to its original temperature. Additionally, the *Yohkoh* SXT observations indicate that some change of magnetic topology occurred in the regions which exhibited emission depletion, which gives additional evidence that the change in EUV emission was not solely due to a shock front propagating through the region.

The observations are not sufficient to distinguish between possible dimming mechanisms. Certainly, the 'plowed up' material in the moving front could consist of evacuated material from the dimming region. The relative changes in emission could support this theory, if we make the poor assumption that the emission recorded in the plasma does not vary with its density or rapid evolution.

In addition to the evidence possibly linking the wave to the coronal mass ejection, the 'traditional' aspects of the Hα and metric type II data (timing, location) still implicate the flare as a possible initiation mechanism. Additionally, the formation of the dimming also appears to emanate from the flaring site. The location of the flare seems central to all of the associated phenomena.

The metric radio type II bursts began at 02:47 UT and continued until approximately 02:59 UT. As mentioned previously, an Hα image obtained at approximately 02:55 UT showed no evidence of the wavefront. By that time, the type II bursts had decreased significantly in frequency, implying that they were occurring at a higher altitude. An Hα image obtained at 02:45 UT indicated that the wave transient had begun developing by that time (though it had not reached its full angular expanse). Smith and Harvey (1971) demonstrated that for the wave observed on September 20, 1963, the type II radio bursts began within 1 minute of the

appearance of the wave transient. Smith and Harvey used these timing arguments to link a number of flare wave transients to a flare origin.

The model developed by Uchida (1968, 1974; Uchida, Altschuler, and Newkirk, 1973) was able to explain both the location and speed of both flare waves and type II bursts. The Uchida model consisted of tracing a fast-mode MHD impulse through a varying coronal density and magnetic field profile. It was shown that the three-dimensional disturbance was focused by areas of low Alfvén speed. The regions where the front intersected the chromosphere reproduced the observed wavefronts quite convincingly.

Based on the Uchida model, however, one would expect the coronal observations to appear spread out over a large area, with an increase in intensity and finer structure where the wavefront was steepening towards the chromosphere. Instead, the coronal observations look very similar to those of the chromosphere, as the location and extent of the EUV sharp front maps quite well with the Hα front. This is not sufficient to exclude the Uchida model, however; a flare occurring close to the edge of an active region (as is this case for this flare) would have an impulse which is refracted towards higher altitudes (and therefore out of EUV visibility) on one side of the flare. Additionally, the model did not rule out the possibility of a directional impulse being delivered by the flare.

The Uchida model is readily applied to recent coronal observations of weak impulses. Typical 'EIT wave' transients appear to be freely propagating and can be observed moving across the entire solar disk. Using high-resolution and high-cadence TRACE EUV data, Wills-Davey and Thompson (1999) show strong evidence of the coronal magnetic field motion as the wave propagates through it, and the guiding of the wave by the magnetic field. Wu *et al.* (1999) have utilized a technique similar to that of Uchida, and have been able to reproduce the propagation and morphology of an 'EIT wave' transient to a stunning degree of accuracy. Neither the Uchida nor the Wu *et al.* model necessarily require that the impulse have a specific initiator; only the existence of the impulse is central to the model.

However, the weak 'EIT wave' transients may be easier to simulate and to reconcile with a weak MHD wave/shock model. Again, the high-amplitude limit of the weak waves may have an appearance similar to those observed in the 24 September 1997 data. One possible explanation for the appearance of coronal dimming regions is rapid heating by the shock transit, and many of the features of the observations can be incorporated by slight modifications of the MHD models.

An entirely different approach also shows promise. The model described by Delannée and Aulanier (1999) provides a mechanism by which a coronal mass ejection which is triggered by a flare reconnection can produce a bright arc-shaped EUV 'front.' They report the observation of a bright arc in the EIT data which apparently remains stationary for more than 10 min; this arc also appears in conjunction with coronal dimming regions, but clearly cannot be wave-like in nature because it does not propagate. Furthermore, the identification of a transient as a 'wave' implies that its propagation involves the transfer of information through a

medium; simple material motion, or a series of brightenings which are caused by a non-propagating disturbance should be excluded from classification as a wave.

The Delannée and Aulanier model predicts both the location of EUV brightenings as the result of opening magnetic fields lines in a CME. The dimming regions are regions predicted by their model to be depleted by the eruption, and consist of areas both close to the flaring region and other areas (including near other active regions) which are magnetically connected by loops overlaying the flaring region. The events described have three pieces of evidence supporting this theory: first, dimmings occur near the flaring region and also additional dimmings are observed north of the equator near active region No. 8089. Second, both of the observed EUV sharp wavefronts on 24 September 1997 occur roughly at the edge of the dimming region closest to the flaring active region, suggesting the location of a separatrix in the model. Finally, the *Yohkoh* SXT data show evidence of post-eruption arcades also extending over this area, possibly indicating a change in magnetic topology. The model proposes that an observed propagation of the wavefront (or arc-shape) may come from the consecutive opening of field lines and the resulting compression of material.

Unfortunately, both the MHD approach and the opening magnetic field line approach are both able to adequately explain many features of the 24 September 1997 observations, and we are unable to eliminate either model from consideration, and are similarly left with the same question of whether coronal shock waves are piston-driven or blast waves. However, the presence of both sharp and diffuse wavefronts, as well as evidence that both the CME and the flare are essential aspects of the observations, may cause us to return to an old lesson eventually learned by anyone studying the Sun: posing a question by attempting to differentiate between one thing *or* another can drastically impede your ability to assess the relative contribution of *both*.

Acknowledgements

BJT would like to gratefully acknowledge discussions with Y. Uchida, C. Delannée, G. Aulanier, M. Wills-Davey, and E. Cliver. NG is an NAS/NRC Senior Research Associate.

References

Athay, R. G. and Moreton, G. E.: 1961, *Astrophys. J.* **133**, 935.
Bougeret, J.-L. *et al.*: 1995, *Space Sci. Rev.* **71**, 231.
Brueckner, G.E. *et al.*: 1995, *Solar Phys.* **162**, 357.
Cane, H. V.: 1983, in M. Neugebauer (ed.), *Solar Wind Five*, p. 703.
Cliver, E. W.: 1999, *J. Geophys. Res.* **104, A3**, 4743.
Cliver, E. W., Webb D. F., and Howard, R. A.: 1999, *Solar Phys.* **187**, 89.

Delaboudinière, J.-P. *et al.*: 1995, *Solar Phys.* **162**, 291.
Delannée, C. and Aulanier, G.: 1999, *Solar. Phys.* **190**, 107.
Dodson, H. W.: 1949, *Astrophys. J.* **110**, 382.
Dodson, H. W., Hedeman, E. R., and Chamberlain, J.: 1953, *Astrophys. J.* **117**, 66.
Gopalswamy, N., Kaiser, M. L., Lepping, R. P., Kahler, S. W., Ogilvie, K., Berdichevsky, D., Kondo, T., Isobe, T., and Akioka, M.: 1998, *J. Geophys. Res.* **10**, 307.
Hudson, H. S., Acton L. W., and Freeland, S. L.: 1996, *Astrophys. J.* **470**, 629.
Hudson, H. S. and Webb, D.: 1997, in Crooker, Joselyn, and Feynman (eds), *Coronal Mass Ejections*, American Geophysical Union Geophysical Monograph 99.
Kai, K.: 1970, *Solar. Phys.* **11**, 310.
Klassen, A., Aurass, H., Klein, K.-L., Hofmann, A., and G. Mann, G.: 1999, *Astron. and Astrophys.* **343**, 287.
Klassen, A., Aurass, H., Mann G., and Thompson, B. J.: 2000, *Astron. Astrophys.*, in press.
Krucker, S., Larson, D., Lin R., and Thompson, B. J.: 1999, *Astrophys. J.* **519**, 864.
Mann, G.: 1995, in A. O. Benz and A. Krüger (eds), *Lecture Notes in Physics 44, Coronal Magnetic Energy Releases*, Springer-Verlag, Berlin, p. 183.
Mann, G., Aurass, H., Voigt, W., and Paschke, J.: 1992, ESA-Journal, SP-348, 129.
Mann, G., Jansen, F., MacDowall, R. J., Kaiser, M. L., Stone, R. G.: 1999, *Astron. Astrophys.* **348**, 614.
Maxwell, A. and Thompson, A. R.: 1962, *Astrophys. J.* **135**, 138.
Meyer, F.: 1968, in K. O. Kiepenheuer (ed.), 'Structure and Development of Solar Active Regions', *IAU Symp.* **35**, 485.
Moreton, G. E.: 1960, *Astron. J.* **65**, 494.
Moreton, G. E. and Ramsey, H. E.: 1960, *Publ. Astron. Soc. Pacific* **72**, 357.
Moreton, G. E.: 1965, in 'Stellar and Solar Magnetic Fields', *IAU Symp.* **22** 371.
Newkirk, G.: 1961, *Astrophys. J.* **133**, 983.
Nitta, N. and Akiyama, S.: 1999, *Astrophys. J.* **525**, L57.
Pick, M., Maia, D., Vourlidas, A., Benz, A. O., Howard, R. A., and Thompson, B. J.: 1999, in S. R. Habbal, R. Esser, J. V. Hollweg, and P. A. Isenberg (eds), *Solar Wind Nine: Proceedings of the Ninth International Solar Wind Conference*, American Institute of Physics, 649.
Pinter, S.: 1977, Spec. Rep. AFGL-SR-209, Hanscom Air Force Base, 35.
Ramsey, H. E. and Smith, S. F.: 1966, *Astron. J.* **71**, 197.
Richardson, R. S.: 1936, Annual Report of the Director, Mt. Wilson Obs., Vol. **35**, 871.
Richardson, R. S.: 1951, *Astrophys. J.* **114**, 356.
Roberts, J. A.: 1959, *Australian J. Phys.* **12**, 327.
Robinson, R. D., Stewart R. T., and Cane, H. V.: 1984, *Solar. Phys.* **91**, 159.
Rust, D. M.: 1983, *Space Sci. Rev.* **34**, 21.
Smith, D. F.: 1972, *Astrophys. J.* **174** 163.
Smith, S. F. and Harvey, K. L.: 1971, in C. J. Macris (ed.), *Physics of the Solar Corona*, Reidel Publ. Co., Dordrecht, p. 156.
St. Cyr, O. C. and Plunkett, S. P.: 1999, on-line LASCO CME List.
St. Cyr, O. C. *et al.*: 1999, *J. Geophys. Res.*, in preparation.
Sterling, A. C. and Hudson, H. S.: 1997 *Astrophys. J.* **491**, L55.
Thompson, B. J., Plunkett, S. P., Gurman, J. B., Newmark, J. S., St. Cyr, O. C., Michels, D. J., and Delaboudinière, J.-P.: 1998, *Geophys. Res. Lett.* **25**, 246.
Thompson, B. J., Newmark, J. S., Gurman, J. B., Neupert, W., Delaboudinière, J.-P., St. Cyr, O. C., Stezelberger, S., Dere, K. P., Howard, R. A., and Michels, D. J.: 1999, *Astrophys. J.* **517**, L151.
Thompson, B. J., Cliver, E. W., Nitta, N., Delannée, C., and Delaboudinière, J.-P.: 2000, *Geophys. Res. Lett.*, submitted.
Torsti, J., Kocharov, L., Teittinen, M., and Thompson, B.: 1999, *Astrophys. J.* **510**, L460.
Uchida, Y.: 1968, *Solar Phys.* **4**, 30.

Uchida, Y.: 1970, *Publ. Astron. Soc. Japan* **22**, 341.
Uchida, Y.: 1974, *Solar Phys.* **39**, 431.
Uchida, Y., Altschuler, M. D., and Newkirk G., Jr.: 1973, *Solar Phys.* **28**, 495.
Wagner, W. J. and MacQueen, R. M.: 1983, *Astron. Astrophys.* **120**, 136.
Webb, D. F., Cliver, E. W., Gopalswamy, N., Hudson, H. S., and St. Cyr, O. C.: 1998, *Geophys. Res. Lett.* **25**(14), 2469.
Weiss, A. A.: 1965, *Australian J. Phys.* **18**, 167.
Wild, J. P., Sheridan, K. V., and Neylan, A. A.: 1959, *Australian J. Phys.* **12**, 369.
Wild, J. P., Smerd, S. F., and Weiss, A. A.: 1963, *Ann. Rev. Astron. Astrophys.* **1**.
Wild, J. P.: 1970, *Proc. Astron. Soc. Australia* **1**, 365.
Wills-Davey, M. and Thompson, B. J.: 1999, *Solar. Phys.* **190**, 467.
Wu, S. T. *et al.*: 1999, *Astrophys. J.*, in preparation. 1999.